Environmental Pollution 288 (2021) 117687

Contents lists available at ScienceDirect

Environmental Pollution

journal homepage: www.elsevier.com/locate/envpol

Environmental impact of amino acids on selenate-bearing hydrocalumite: Experimental and DFT studies☆

Mengmeng Wang [a], Hirofumi Akamatsu [b], Ismaila Dabo [c], Keiko Sasaki [a,*]

[a] Department of Earth Resources Engineering, Kyushu University, Fukuoka, 819-0395, Japan
[b] Department of Applied Chemistry, Kyushu University, Fukuoka, 819-0395, Japan
[c] Department of Materials Science and Engineering, The Pennsylvania State University, University Park, PA, 16802, United States

ARTICLE INFO

Keywords:
Selenate
Carbonate
Ca_2Al-LDH
Amino acids
DFT simulation
Chemical bonds

ABSTRACT

Selenium (Se) radioactive wastes can be disposed through stabilization/solidification (S/S) based on the cementitious matrix on hydration products, where hydrocalumite (Ca_2Al-LDH) is expected to play an important role in the retention of SeO_4^{2-}. Natural organic matters (NOMs) are known to be a risk to affect the transportation and mobility of undesirable chemical species in the pedosphere which receives the low level radioactive wastes (LLW). In the present work, five amino acids were selected as the simplified models of NOMs in the pedosphere to explore their effects on the stability of Ca_2Al-LDH after immobilized SeO_4^{2-} under alkaline conditions. As the loading amount of amino acids on Ca_2Al-LDH increasing, release of SeO_4^{2-} was enhanced in HGly, H_2Asp, and H_2Cys series, while no enhancement was observed in HPhe and HTrp series. Density functional theory (DFT) calculation predicted ion-exchange of amino acids and CO_3^{2-} with SeO_4^{2-} in a unit cell of LDH model. The intercalation of Asp^{2-} and CO_3^{2-} caused 003 peaks in XRD sharper and d_{003} decreased from 8.15 Å to 7.70 Å which is assigned to Ca_2Al-LDH(Asp, CO_3). In H_2Cys series, the 003 peaks were kept broad and SeO_4^{2-} was still relatively maintained in LDH which was caused by the lower amounts of intercalated CO_3^{2-} in the presence of H_2Cys. Amino acids in the interlayer of Ca_2Al-LDH have several possible configurations, where the most stable one is prone to be in a horizontal direction through hydrogen bonds and Ca–O chemical bonds. This provides an insight on the stability of selenate immobilized in hydrocalumite, which can be produced in cement disposing in the pedosphere for a long term of burying. Not only carbonate but also small molecular organic matters like amino acids possibly give environmental impact on the mobility of low level anionic radionuclides in LDH.

1. Introduction

Selenium (Se) is a critical micronutrient to the health of living organisms and has a very limited concentration range between deficient and toxic levels (Fordyce, 2013). The accumulation of hazardous Se in the soil environment is derived from disposal of fossil fuel wastes, agricultural irrigation of arid using contaminated water and possibly nuclear power plants leakage (Huang et al., 2009). In the pedosphere, Se dominates in selenate (SeO_4^{2-}) and selenite (SeO_3^{2-}) forms, however, SeO_3^{2-} sorbs in minerals more strongly than SeO_4^{2-} due to the formation of inner-sphere complexes while SeO_4^{2-} is sorbed through weakly bonded outer-sphere complexes and has a lower affinity to oxide mineral surfaces (Baur and Johnson, 2003a; Eklund and Persson, 2014; Guo et al., 2017). Therefore, SeO_4^{2-} has higher mobility than SeO_3^{2-} in the pedosphere, so related removal technologies had been developed. Among them, stabilization/solidification (S/S) for hazardous SeO_4^{2-} polluted soil based on cementitious materials, especially radioactive ^{79}Se wastes, are widely explored involving the mixtures with a binder to reduce the leachability and then convert the Se wastes into an environmentally acceptable form for land disposal.

Low level radioactive wastes (LLW) are sometimes buried in shallow zones of underground with the depth < 10 m, where are some human activities in civil engineering like subways and the foundation of tall buildings. Soil organic matters are constituents in the pedosphere. Unfortunately, the effect of environmental organic matters on the stability of LDH has not yet been paid much attention for the present, while many

☆ This paper has been recommended for acceptance by Bernd Nowack.

* Corresponding author.
E-mail addresses: wang@mine.kyushu-u.ac.jp (M. Wang), h.akamatsu@cstf.kyushu-u.ac.jp (H. Akamatsu), dabo@psu.edu (I. Dabo), keikos@mine.kyushu-u.ac.jp (K. Sasaki).

https://doi.org/10.1016/j.envpol.2021.117687
Received 19 April 2021; Received in revised form 20 June 2021; Accepted 29 June 2021
Available online 5 July 2021

works have been reported for inorganic anionic exchange on hydrocalumite. SeO_4^{2-} is a model of anionic radioactive species of ^{79}Se in the present work, because SeO_4^{2-} is more mobile in nature than SeO_3^{2-} due to less polarity.

Hydrocalumite (Ca_2Al-LDH) is known as one of by-products in cement system, as expressed in the chemical formula as $[Ca_2Al(OH)_2][(A^{n-})_{x/n}{\cdot}yH_2O]$, where A^{n-} is the exchangeable anions like SO_4^{2-}, CO_3^{2-}, Cl^-, NO_3^- incorporating into the interlayer to compensate for positively charged hydroxide layers in contact with aqueous solutions. Ca_2Al-LDH possesses surface adsorption capacity and ion-exchange ability (Perkins and Palmer, 2001; Baur and Johnson, 2003b; Christensen et al., 2004; Moon et al., 2009; Li et al., 2017; Yao et al., 2017). Therefore, Ca_2Al-LDH has been widely explored from aspects of its immobilization mechanisms for Se oxyanion species and phase transformation boundary. Moon et al. (2009) reported selenium-bearing phase appeared calcium selenite hydrate and selenate-ettringite in the soil-cement system. Zhang and Reardon (2003) confirmed that $Ca_4Al_2(OH)_{12}(OH)_2{\cdot}6H_2O$ can reduce SeO_4^{2-} concentration below the drinking water standard and the uptake amount was larger than ettringite. Baur and Johnson (2003b) explored SO_4-monosulfate possibly removes SeO_4^{2-} through substitution with SO_4^{2-} in the cement paste. Li et al. (2020) found the adsorption of SeO_4^{2-} onto Ca–Al LDHs was controlled by the chemisorption and can be reused at least three times with the adsorption capacity still keeping 88%. Yet, the stability of hydrocalumite after immobilized Se oxyanions in the presence of environmental factors is still unknown.

In the pedosphere, there are physical, chemical, and biological factors that might complicatedly affect the immobilization of SeO_4^{2-} in Ca_2Al-LDH. Even though several reports explored the effects of organic substances on the stability of minerals (Evanko and Dzombak, 1998; Besse et al., 2009; Liang and Butler, 2010), there is a few report to describe the role of natural organic matters (NOMs) on the stability of hydrocalumite. Humic substances which are derived from degradation products of animals, microorganisms, and plants occupy more than 50% of NOMs. The molecular structure of humic substances is modeled to include the fragments of protein and sugars which are symbolic of animal and plant cells, respectively. Chen et al. (2016) have demonstrated that humic substances can be removed by Ca_2Al-LDH through anion exchange, ligand exchange, and adsorption on $CaCO_3$, which can be secondarily formed through dissolution of Ca_2Al-LDH. In the structure model of fulvic acids, peptide bonds are often included as their characteristic fragments, suggesting that amino acids can be released to the pedosphere in the degradation process of animal tissues. Proteins are organized by polymerization of naturally occurring 20 types of amino acids. Each amino acid molecule contains amino (-NH_2) and carboxyl (-COOH) groups at least one for each, furthermore, along with the side chain and acid dissociation constants (pK_a) specific to each amino acid making them possess different properties. Under alkaline conditions, they are negatively charged on conjugated bases. Amino acids are very simplified models to facilitate DFT works as well as experimental works here. We selected five amino acids in different molecular sizes, charge densities, and functional groups to explore the stability of SeO_4^{2-} in hydrocalumite. LDHs are also versatile materials and can be functionalized by amino acids complexes for catalysts in dehydration, oxidation, etherification, and so on (Sipos and Pálinkó, 2018), where LDHs act as nano-reactors. This suggests amino acids might stabilize LDHs, possibly affecting the mobility of existing SeO_4^{2-}. Therefore, their environmental effects of amino acids on the stability of Ca_2Al-LDH after immobilized SeO_4^{2-} attracted our attention.

Considering the real environmental factors in cement systems and the practical purity of SeO_4-hydrocalumite, selenate- and carbonate-bearing hydrocalumite (Ca_2Al-LDH) was obtained by co-precipitation method in the present work. Five amino acids were selected to react with it. Releasing concentrations of SeO_4^{2-} from Ca_2Al-LDH after suspended into amino acids solutions were determined and sorption isotherms of the amino acids were obtained. XRD patterns of Ca_2Al-LDH solid residues were analyzed through peak separation to give the peak assignments assisted by DFT simulation. Also, DFT was applied to predict the possible mechanisms to release SeO_4^{2-} and possible interactions of amino acids with hydroxide layers of Ca_2Al-LDH.

2. Experimental

2.1. Sample preparation

Inorganic chemicals including $Ca(OH)_2$ (96.0%), $NaAlO_2$ (Al_2O_3 > 42.0%), Na_2SeO_4 (97.0%), NaOH (97.0%) and organic chemicals including L-tryptophan (HTrp, $C_{11}H_{12}N_2O_2$, 99.0%), L-phenylalanine (HPhe, $C_9H_{11}NO_2$, 99.0%), glycine (HGly, $C_2H_5NO_2$, 99.0%), L-aspartic acid (H_2Asp, $C_4H_7NO_4$, 99.0%) and L-cysteine (H_2Cys, $C_3H_7NO_2S$, 99.0%) in a special grade were purchased from FUJIFILM Wako Pure Chemicals Co. Ltd. (Osaka, Japan). Decarbonized water was prepared by simultaneously boiling the ultrapure water under the N_2 bubbling for 2 h.

Selenate-bearing hydrocalumite (Ca_2Al-LDH) was prepared by co-precipitation method. First, 0.012 mol $NaAlO_2$ was dissolved into 50 mL 10 mM Na_2SeO_4 for 10 min (solution A). $Ca(OH)_2$ suspension was prepared using 0.024 mol $Ca(OH)_2$ dissolved in 200 mL 10 mM Na_2SeO_4 (solution B). Then solution A was added into solution B to react for 1 h to avoid the SeO_4-ettringite formation in a glovebox (95% N_2, 5% H_2, COY, M-160, USA). After washing 2 times by ultrapure water and freeze-drying for 12 h, powdery Ca_2Al-LDH was obtained and stored inside the drying shelf for further use.

2.2. Reaction of Ca_2Al-LDH with and without amino acids

First, 50 mg of Ca_2Al-LDH was added into 50 mL decarbonized water at pH 11.0 without any amino acids to shake for an appropriate time from 0.5 h to 24 h at 25 °C. The suspensions were collected at different time intervals using disposable syringes and solid residues were separated by filtration using 0.2 μm membrane filters, and then drying solid samples for further characterization. The remaining Ca^{2+}, $Al(OH)_4^-$, and SeO_4^{2-} concentrations in the solution were determined by an inductively coupled plasma optical emission spectrometry (ICP-OES, Optima 8300, PerkinElmer, USA). The dissolved fraction of SeO_4^{2-} was calculated by Eq. (1).

$$\text{Dissolution } (\%) = Q_t \bullet 100/Q_0 \quad (1)$$

where the Q_0 (mmol/g) and Q_t (mmol/g) are the initial amount and final amount at t h of SeO_4^{2-}, respectively.

Then, the reaction of Ca_2Al-LDH with different amino acids including HPhe, HTrp, HGly, H_2Asp, and H_2Cys at a concentration range from 0 to 7 mM was performed in a glovebox to avoid contamination from CO_2. 50 mg of Ca_2Al-LDH was added into 50 mL of the above sole amino acid solution for 24 h at 25 °C. The solution and solid samples were collected in the same manner as above to provide for the determination of dissolved species concentrations and solid characterization, respectively.

2.3. Characterizations

Chemical compositions of the synthesized Ca_2Al-LDH were estimated by ICP-OES after acid dissolution for metal contents and CHN analyzer (CHN MT-5, Yanaco, Kyoto, Japan) for C contents in all of the solid residues. Amino acids concentrations were determined using high-performance liquid chromatography (HPLC, JASCO LC-Net II/ADC, Hachioji, Japan) with a column (Shim-pack GIST-HP C18 column, Shimadzu, Kyoto, Japan) and a UV detector (UV-2075 plus, JASCO, Hachioji, Japan). XRD patterns of solid residues were collected on X-ray diffraction by RIGAKU Ultima IV XRD (Akishima, Japan) using Cu Kα radiation (40 kV, 40 mA) at a scanning speed of 2° min^{-1} and with a scanning step of 0.02°. Peak separation of XRD results was performed by the software package of PeakFit Ver.4.12 (Systat Software, Inc, USA).

2.4. DFT simulation

Our density functional theory (DFT) simulation was performed to calculate the formation energies of the products in ion-exchanges of SeO_4^{2-} with amino acids and of CO_3^{2-} with amino acids by changing the reacted fractions. Considering the equivalent negative charges with SeO_4^{2-}, H_2Asp and H_2Cys were selected as amino acids models in the present work to figure out their ion-exchanging ability depending on the formation energies and the possible configurations of Ca_2Al-LDH including different anions.

The projector augmented-wave (PAW) method (Blöchl, 1994; Kresse and Joubert, 1999) implemented in the VASP code (Kresse and Hafner, 1993a, 1993b; Kresse and Furthmüller, 1996a, 1996b) was employed for precise description of electronic structures and low computational costs. The PBEsol-type of exchange-correlation functional within the generalized gradient approximation (GGA) (Perdew et al., 1996, 1997, 2008) combining with D3 van der Waals correction (Grimme et al., 2010, 2011) was used with the plane-wave cutoff energy of 550 eV. We treated the following states as valence electrons: 1s for H; 2s and 2p for C, N, and O; 3s and 3p for Al and S; 3p and 4s for Ca; 4s and 4p for Se.

Initial structural models were prepared as follows. Firstly, the structural model of positively charged hydroxides layers for Ca_2Al-LDH was constructed for the computer simulation. The hydroxide layers of Ca_2Al-LDH used in the simulations were set using atomic coordinates extracted from the previously reported crystal structure of hydrocalumite with the composition of $[Ca_8Al_4(OH)_{24}(CO_3)(Cl)_2{\cdot}10H_2O]$ (Sacerdoti and Passaglia, 1988). By removing the intercalated carbonate (CO_3^{2-}) and chloride (Cl^-) ions and water (H_2O) molecules, an "empty" LDH model was created. Since the composition of the LDH layer is $[Ca_2Al(OH)_6]^+$, the number of Al atom corresponds to the positive charge of the empty LDH model. Secondly, SeO_4^{2-}, CO_3^{2-}, Asp^{2-} and Cys^{2-} anions are placed in the gallery space of the empty LDH with random positions and rotation angles by using the pymatgen python library (Ong et al., 2013) so as to neutralize the positive charges. Thus, more than ten simulated unit cells consisting of the positively charged hydroxide layers of $[Ca_2Al(OH)_6]^+$ and desired intercalated anions were constructed.

Relaxation of lattice constants and internal coordinates was performed until the residual stress and force decreased to 4 MPa and 1 meV/Å, respectively. The pymatgen python library was used to extract the structural information such as interlayer spacing and the number of chemical bonds from the optimized structures (Ong et al., 2013). The VESTA code was used to visualize the optimized structures (Momma and Izumi, 2011).

Formation energies of the reaction products and reactants should be a good index to predict the most possible reaction in a molecular level by DFT. The total energies of the Ca_2Al-LDH incorporating the anions as well as those of H_2Asp, H_2Cys, H_2SeO_4, and H_2CO_3 neutral molecules were calculated to obtain the formation energies of the products in ion-exchange of SeO_4^{2-} and CO_3^{2-} with Asp^{2-} and Cys^{2-} as expressed as Eqs. (2)–(5), where the values of x are 0, 0.5, and 1.

$$Ca_2Al(OH)_6{\cdot}0.5(SeO_4)+0.5xH_2Asp \rightarrow Ca_2Al(OH)_6{\cdot}0.5(1\text{-}x)\ SeO_4{\cdot}0.5xAsp+0.5xH_2SeO_4 \quad (2)$$

$$Ca_2Al(OH)_6{\cdot}0.5(SeO_4)+0.5xH_2Cys \rightarrow Ca_2Al(OH)_6{\cdot}0.5(1\text{-}x)SeO_4{\cdot}\ 0.5xCys+0.5xH_2SeO_4 \quad (3)$$

$$Ca_2Al(OH)_6{\cdot}0.5(CO_3)+0.5xH_2Asp \rightarrow Ca_2Al(OH)_6{\cdot}0.5(1\text{-}x)\ CO_3{\cdot}0.5xAsp+0.5xH_2CO_3 \quad (4)$$

$$Ca_2Al(OH)_6{\cdot}0.5(CO_3)+0.5xH_2Cys \rightarrow Ca_2Al(OH)_6{\cdot}0.5(1\text{-}x)\ CO_3{\cdot}0.5xCys+0.5xH_2CO_3 \quad (5)$$

Moreover, ion-exchanging of SeO_4^{2-} in ternary anionic systems (SeO_4^{2-}/CO_3^{2-}/amino acid) was also explored to predict the effect of CO_3^{2-} on the release of SeO_4^{2-} from Ca_2Al-LDH in the presence of amino acids. Formation energies of the products in Eqs. (6), (7) were simulated at $x = 0$ and 0.5.

$$Ca_2Al(OH)_6{\cdot}0.5(0.5SeO_4{\cdot}0.5Asp)+0.5xH_2CO_3 \rightarrow Ca_2Al(OH)_6{\cdot}0.5((0.5\text{-}x)\ SeO_4{\cdot}0.5xCO_3{\cdot}0.5Asp)+0.5xH_2SeO_4 \quad (6)$$

$$Ca_2Al(OH)_6{\cdot}0.5(0.5SeO_4{\cdot}0.5Cys)+0.5xH_2CO_3 \rightarrow Ca_2Al(OH)_6{\cdot}0.5((0.5\text{-}x)\ SeO_4{\cdot}0.5xCO_3{\cdot}0.5Cys)+0.5xH_2SeO_4 \quad (7)$$

3. Results and discussion

3.1. Characterization of synthesized Ca_2Al-LDH

The chemical formula of Ca_2Al-LDH in a composition of $Ca_{0.872}Al_{0.402}(OH)_{2.6}(SeO_4)_{0.093}(CO_3)_{0.063}{\cdot}10H_2O$ was obtained by combining with ICP-OES and CHN analytical results, indicating the molar ratio of Ca/Al is 2.17. Considering the difficulty to synthesize pure selenate-bearing hydrocalumite, SeO_4^{2-} and CO_3^{2-} co-intercalated hydrocalumite was obtained. The reagent $NaAlO_2$ in which $NaCO_3$ seems to be contained as an impurity caused the CO_3^{2-} as an intercalator for the produced LDH.

Fig. 1(a) shows the XRD pattern of synthesized Ca_2Al-LDH. The interlayer spacing at d_{003} was 8.15 Å which was consistent with the previous reports by experimental studies (Baur and Johnson, 2003b; Baur et al., 2004). Two weak peaks of portlandite $Ca(OH)_2$ (PDF # 72–0156) were also detected around 18.1° and 34.8° in 2θ. Due to the existence of CO_3^{2-} derived from air, peak separation of 003 plane in Fig. 1(a) was carried out as shown in Fig. 1(b). There are four peaks correspond to components (A), (B), (C), and (D). Component (A) with d_{003} = 7.93 Å was assigned to Ca_2Al-LDH (unknown) where the interlayer should include SeO_4^{2-} and CO_3^{2-} possibly as intercalators. According to previously reports (Baur and Johnson, 2003b; Zhang and Reardon, 2003), components (B) with d_{003} = 8.11 Å, (C) with d_{003} = 8.31 Å, and (D) with d_{003} = 9.81 Å were assigned to Ca_2Al-LDH(SeO_4) but with different water molecule numbers in hydration of SeO_4^{2-} in Ca_2Al-LDH interlayer.

3.2. Suspension of Ca_2Al-LDH in alkaline solution

Changes in the released SeO_4^{2-}, Ca^{2+}, and $Al(OH)_4^-$ concentrations over time are shown in Fig. 2(a)–(c) when the synthesized Ca_2Al-LDH was suspended into alkaline solutions without any amino acids. Simple dissolution caused 0.34 mM SeO_4^{2-} released from Ca_2Al-LDH within 15 min, then the concentration gradually raised to 0.45 mM at the equilibrium around 6 h, where 4.4 mM Ca^{2+} and 1.8 mM $Al(OH)_4^-$ were dissolved. The pH values immediately increased from 11.0 to 12.0 (Fig. 2(d)). This means Ca_2Al-LDH is much more fragile than Mg_2Al-LDH which in our previous report (Wang et al., 2021).

Fig. 1(c) shows the changes in XRD patterns of the solid residues at different suspending time intervals in the absence of amino acids. After 15 min, the main peak position (003 plane) of Ca_2Al-LDH shifted from 10.7° to 9.14° in 2θ corresponding to the interlayer spacing expanded from 8.15 Å to 9.66 Å. The peak intensity at 9.14° in 2θ increased from 15 min to 6 h and then partially shifted to 11.0° in 2θ after 12 h. The dominant interlayer spacing of Ca_2Al-LDH in the solid residues was always kept around 9.66 Å which is probably due to the hydration of SeO_4^{2-} in interlayer without amino acids. Also, the interlayer spacing of Ca_2Al-LDH(SeO_4) is strongly dependent on the number of coordinated water molecules.

The bond length of Se–O in SeO_4^{2-} is around 1.644 Å and it can possess various bond length values when combined with different numbers of water molecules in the aqueous solution. It has been reported that the Se–O bond length was 1.674 Å for hexa-hydrated selenate, however, the length is changeable from 1.655 to 1.701 Å for trihydrated selenate (Pye and Walker, 2011; Eklund and Persson, 2014).

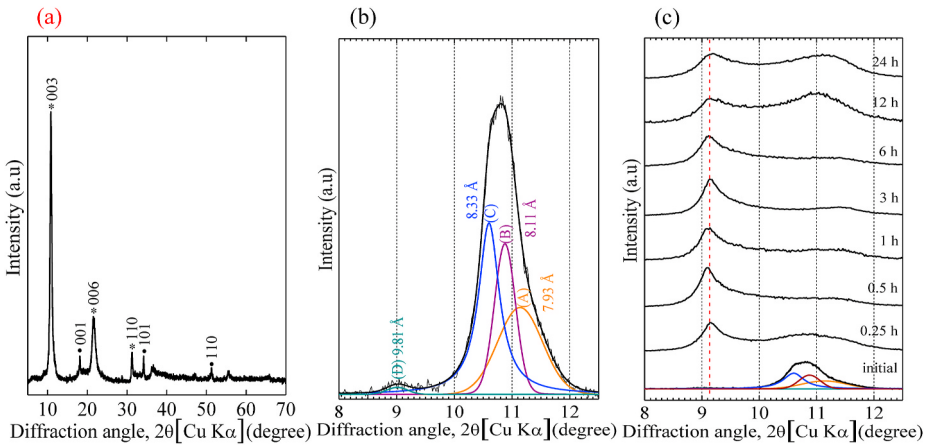

Fig. 1. X-ray diffraction patterns of synthesized Ca2Al-LDH in a region of (a) 5°–70°, (b) 8° to 12.5° in 2θ, (c) changes in XRD patterns of Ca2Al-LDH over suspending time in alkaline solutions. Symbols in (a): *, Ca_2Al-LDH (PDF#42–0063); ●, $Ca(OH)_2$ (PDF#72–0156) and in (b): (A), Ca2Al-LDH (unknown); (B)~(D), Ca2Al-LDH(SeO4).

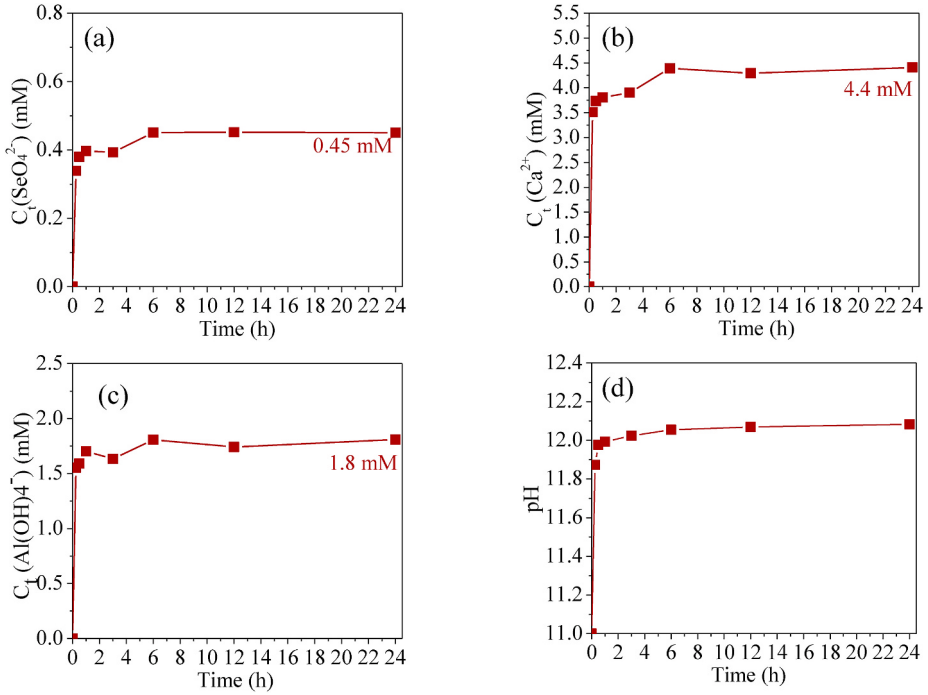

Fig. 2. Dissolution kinetics of (a) SeO_4^{2-}, (b) Ca^{2+}, and (c) $Al(OH)_4^-$ concentrations from synthesized Ca_2Al-LDH and (d) pH after suspended into alkaline solutions without amino acids.

Therefore, when SeO_4^{2-} is hydrated in LDH, the Se–O bond length tends to increase to different extents and is possible to expand the interlayer spacing of Ca_2Al-LDH.

3.3. Interaction of Ca_2Al-LDH with amino acids

After adding the synthesized Ca_2Al-LDH into amino acids solutions at pH 11.0, the releasing behaviors of SeO_4^{2-}, Ca^{2+} and $Al(OH)_4^-$ showed different trends compared with the blank test. As shown in Fig. 3(a), with increase in the concentrations of HPhe and HTrp to 5.0 mM, the released concentration of SeO_4^{2-} was maintained around 0.47 mM which is close to in the blank, indicating that the HPhe and HTrp did not promote the release of SeO_4^{2-} from Ca_2Al-LDH. On the other hand, HGly, H_2Asp, and H_2Cys enhanced SeO_4^{2-} releasing progressively with an increase in the concentrations, compared with in the blank (C_0 for amino acid = 0). The equilibrated SeO_4^{2-} concentrations reached 0.687 mM in H_2Asp, 0.623 mM in HGly, and 0.592 mM in H_2Cys which correspond to 73.8%, 66.9% and 63.7% in the original contents of SeO_4^{2-} in LDH. In the presence of amino acids, the release of Ca^{2+} and $Al(OH)_4^-$ was lower than in the blank test, suggesting that amino acids might inhibit the dissolution of hydroxide layer of Ca_2Al-LDH through surface adsorption (Fig. 3(b), (c)). HPhe and HTrp molecules have one amino and one carboxyl group with an aromatic group in a side-chain that possesses the hydrophobic property. Under alkaline conditions, HPhe and HTrp are deprotonated to be Phe^- and Trp^- because of the pK_a values of carboxyl groups. However, ion-exchange of SeO_4^{2-} with Phe^- and Trp^- in interlayer spaces did not happen significantly, probably due to their larger molecular sizes and hydrophobicity. H_2Asp, H_2Cys, and HGly are relatively hydrophilic amino acids, where H_2Asp and H_2Cys are dissociated to Asp^{2-}, Cys^{2-} under alkaline conditions to cause the same negative charge numbers with SeO_4^{2-}. While HGly would get one negative charge but it has the smallest molecular size making it more easily intercalated

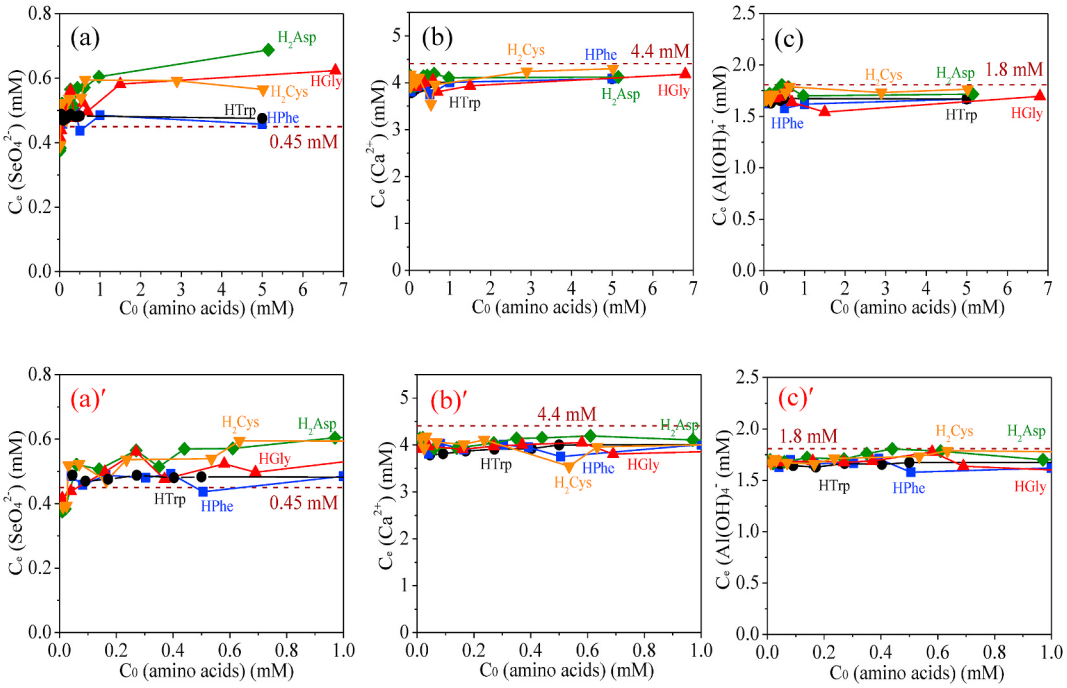

Fig. 3. Plots of (a) SeO42-, (b) Ca2+, and (c) Al(OH)4- dissolved concentrations from Ca2Al-LDH against the initial amino acid concentrations. The x axis was expended in a range of 0–1 mM in (a)', (b)', and (c)'. Dotted lines indicate the equilibrated concentrations in the absence of amino acids ($C0 = 0$).

into Ca_2Al-LDH. Based on the above properties of each amino acid molecule, HGly, H_2Asp, and H_2Cys might have promoted the release of SeO_4^{2-} from Ca_2Al-LDH interlayer through ion-exchange, this behavior affects the stability of SeO_4^{2-} in Ca_2Al-LDH.

Since the partial dissolution happened with Ca_2Al-LDH, the sorption data of amino acids onto Ca_2Al-LDH were fitted to Freundlich model (Eq. (8)) rather than Langmuir model, as shown in Fig. 4.

$$Q_e = K_f C_e^{\,1/n} \tag{8}$$

where C_e (mM) is the equilibrium concentration, Q_e (mmol/g) is the adsorption density, K_f represents the adsorption capacity, $1/n$ represents the adsorption intensity ($0 < 1/n < 1$). Fitting results are summarized in Table S1. The Freundlich sorption constants (K_f) were in the order of HGly > H_2Cys > H_2Asp > HTrp > HPhe, indicating that HGly has a significantly higher affinity than other amino acids, especially compared with HPhe and HTrp (Yan et al., 2009; Cheng et al., 2010). The molecular size is more important to affect the intercalation than charge numbers, probably due to the different steric hindrance they caused (Santos et al., 2017). In HGly, H_2Asp, and H_2Cys series, they showed high adsorption densities which might be contributed by their intercalation. This also implies that the possible mechanism to enhance SeO_4^{2-} release from Ca_2Al-LDH by HGly, H_2Asp, and H_2Cys might be a partial substitution with SeO_4^{2-} in the interlayer.

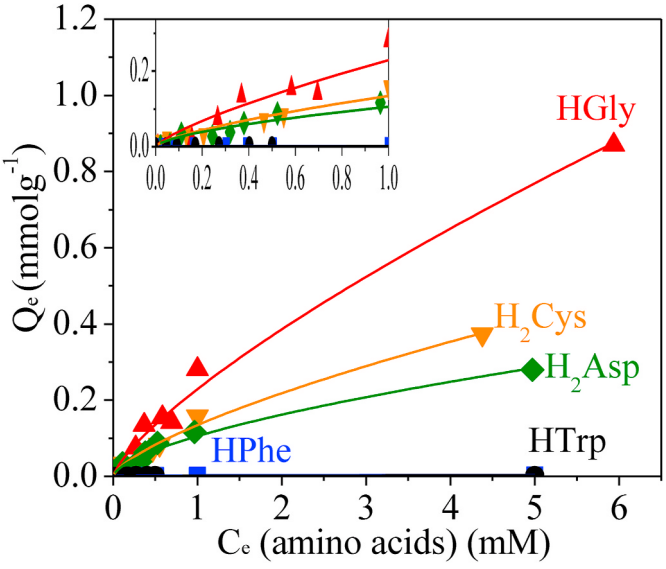

Fig. 4. Sorption isotherms of HGly (▲), H2Asp (◆), H2Cys (▼), HPhe (■), and HTrp (●) onto Ca2Al-LDH. Solid lines indicate the fittings to Freundlich model.

3.4. XRD peak separation at d_{003} for Ca_2Al-LDH solid residues

XRD patterns of each solid residue of Ca_2Al-LDH after interacting with different amino acids were collected and its peak separation was performed to explore the effect of amino acids on the stability of SeO_4^{2-} in Ca_2Al-LDH as shown in Fig. 5. XRD patterns for Ca_2Al-LDH after interacted with HGly, H_2Asp, and H_2Cys series were changed depending on the initial amino acids concentrations (Fig. 5(a)–(c)). As the loading amount of amino acids increasing, the 003 peak position was shifted to larger angles in 2θ gradually. In all XRD patterns except for H_2Asp-1 (Fig. 5(b)), the largest layer spacing component at d_{003} = 9.81 A (component (D)) disappeared while it was observed clearly in the blank test (Fig. 1(c)). Due to the relatively large adsorption amounts of HGly, H_2Asp, and H_2Cys in Ca_2Al-LDH (Fig. 4) and their enhanced leaching effects on SeO_4^{2-} (Fig. 3), amino acids should be considered as one of the intercalators in peak separation process. In the low concentration range of amino acids (0.00–0.03 mM), the adsorption amount of them almost can be ignored as shown in Fig. 4, hence, the intercalation of HGly, H_2Asp, and H_2Cys into Ca_2Al-LDH seemed not occur in this range. Taking this into consideration, the separation of 003 peak in Fig. 5(a)–(c) was carried out in the same manner as the original material (Fig. 1 (b)) which only include the component of Ca_2Al-LDH(unknown) and Ca_2Al-LDH(SeO_4). As the concentrations of amino acids increasing to $[HGly]_0$ > 0.16 mM (HGly-3), $[H_2Asp]_0$ > 0.06 mM (H_2Asp-3), and $[H_2Cys]_0$ > 0.03 mM (H_2Cys-3), the main peak position started shift to

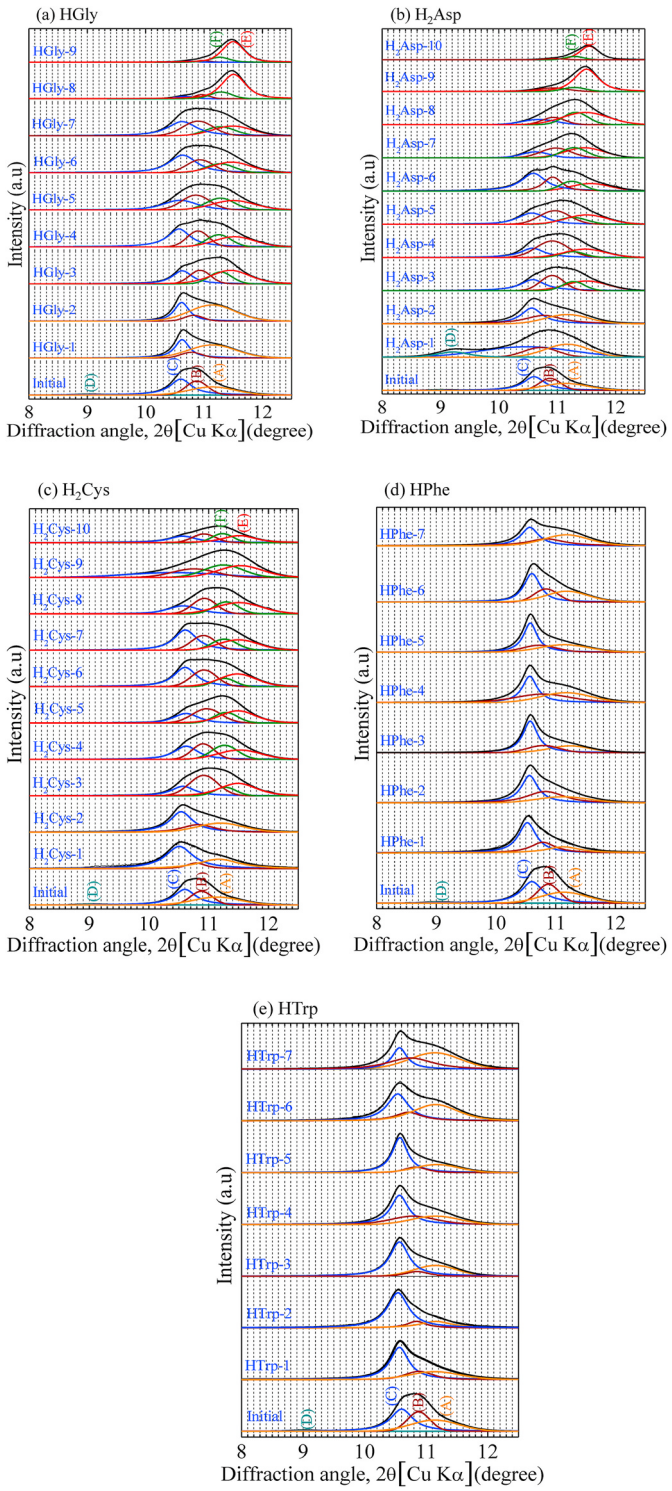

Fig. 5. X-ray diffraction patterns of Ca2Al-LDH solid residues after suspended in different concentrations of amino acids. Component E, Ca2Al-LDH(amino acid, CO3) ($d003$ = 7.70 Å); F, Ca2Al-LDH(amino acid) ($d003$ = 7.83 Å); A, Ca2Al-LDH(unknown) ($d003$ = 7.93 Å); B, Ca2Al-LDH(SeO4) ($d003$ = 8.11 Å); C, Ca2Al-LDH)(SeO4) ($d003$ = 8.31 Å) and D, Ca2Al-LDH(SeO4) ($d003$ = 9.81 Å).

larger diffraction angles. Also, the adsorption amount of them started increasing, there appeared two additional components after the separation of d_{003} with interlayer spacing in 2θ which present as component (E) with 7.70 Å (11.5°, 2θ) and component (F) with 7.83 Å (11.28°, 2θ). Components of (B) and (C) were identified in the original material, but the peak assignment of (A), (E), and (F) are still unclear. At the highest concentrations of HGly and H_2Asp, component (E) seems to have become the predominant phase which indicates the main intercalator has been transited from SeO_4^{2-} to other anions.

XRD patterns for the solid residues after suspension of Ca_2Al-LDH in 0–5 mM HPhe and HTrp did not show the components (D), (E), and (F) at all. Considering the trace amount of adsorption of HPhe and HTrp in Ca_2Al-LDH (as shown in Fig. 4), the intercalation of HPhe and HTrp should not be considered in the peak separation of XRD patterns for the solid residues. Therefore, there were still three components (A), (B), (C) of 003 reflections in all of XRD patterns as depicted in Fig. 5(d), (e), which are the same as original material. Based on the peak assignment in Fig. 1(b), the components of (B) and (C) are assigned to Ca_2Al-LDH (SeO_4) (d_{003} = 8.11 Å) and Ca_2Al-LDH(SeO_4) (d_{003} = 8.31 Å) with different hydrations, and the component (A) is assigned to Ca_2Al-LDH (unknown) (d_{003} = 7.93 Å).

For a better understanding of the components of (E) and (F), which were observed in Fig. 5(a)–(c), DFT simulations were performed. Since there are similar trends in changes of XRD patterns between HGly and H_2Asp series but different from H_2Cys series, anions of Asp^{2-}, Cys^{2-}, SeO_4^{2-} and CO_3^{2-} in solutions were selected to simulate the possible interactions among anions in Ca_2Al-LDH and the corresponding interlayer spacings as well as formation energies. Under the present alkaline condition, H_2Asp and H_2Cys were dissociated to be Asp^{2-} and Cys^{2-}. In the unit cell of $Ca_2Al(OH)_6{\cdot}0.5SeO_4$, the ion-exchange of amino acids with SeO_4^{2-} was simulated in Fig. 6(a), (b). Atomic and electronic structure calculations predicted that SeO_4^{2-} is preferable to remain in the interlayer of Ca_2Al-LDH than Asp^{2-} and Cys^{2-} because the greater x values lead to the larger formation energies. Since CO_3^{2-} also was included in the unit cell of $Ca_2Al(OH)_6{\cdot}0.5CO_3$, the ion-exchange of Asp^{2-} and Cys^{2-} with CO_3^{2-} also was calculated by changing x values as shown in Fig. 6 (c), (d). In the unit cell of $Ca_2Al(OH)_6{\cdot}0.5(1\text{-}x)CO_3{\cdot}0.5x$Asp at $x = 1$ after intercalation of Asp^{2-}, the formation energies were lower than $Ca_2Al(OH)_6{\cdot}0.5(1\text{-}x)CO_3{\cdot}0.5x$Cys at $x = 1$. This indicates that Asp^{2-} can be more easily ion-exchanged than Cys^{2-}, and that Asp^{2-} is likely to occupy the adsorption sites in the interlayer of Ca_2Al-LDH than CO_3^{2-}. Therefore, based on the above results, the selectivity of ion-exchange sites in Ca_2Al-LDH interlayer can be expected in the order of $SeO_4^{2-} > Asp^{2-} > Cys^{2-} \cong CO_3^{2-}$.

Regarding possible combinations of a couple of anions in the unit cell of $Ca_2Al(OH)_6(X, Y)$ including different configurations of amino acids, SeO_4^{2-} and CO_3^{2-}, the distribution of interlayer spacing values in angstrom (Å) were obtained as shown in Fig. 7. When the single anion exists in one unit cell, there were four systems of Ca_2Al-LDH including $Ca_2Al(OH)_6{\cdot}0.5$Asp,$Ca_2Al(OH)_6{\cdot}0.5$Cys, $Ca_2Al(OH)_6{\cdot}0.5CO_3$, and $Ca_2Al(OH)_6{\cdot}0.5SeO_4$.

For $Ca_2Al(OH)_6{\cdot}0.5$Asp and $Ca_2Al(OH)_6{\cdot}0.5$Cys, the calculated d values were distributed in wider ranges of interlayer spacing of 7.3–9.5 Å and 7.2 to 9.0 Å (Fig. 7(a),(d)), respectively, than inorganic anions intercalated LDH (Fig. 7(g)–(i)). Amino acids molecules can be in a large variety of configurations in LDH interlayers due to mostly consisting of single bonds, which affects the interlayer spacing. H_2Asp possesses a larger molecular size than H_2Cys, which is consistent with the results in Fig. 7(a),(d). Regarding SeO_4^{2-} and CO_3^{2-}, CO_3^{2-} has a smaller ionic radius than SeO_4^{2-} which can be also seen in XRD patterns for $Ca_2Al(OH)_6{\cdot}0.5CO_3$ (Fig. 7(i)) and $Ca_2Al(OH)_6{\cdot}0.5SeO_4$ (Fig. 7(h)), showing a relatively narrow range of interlayer spacing with 6.2–6.5 Å and 7.5 to 8.1 Å, respectively. When the mixed anions exist in one unit cell (x = 0.5), including one type of amino acid, four systems were considered to calculate. In the unit cells of $Ca_2Al(OH)_6{\cdot}0.5(1\text{-}x)SeO_4{\cdot}0.5x$Asp ($x = 0.5$) and $Ca_2Al(OH)_6{\cdot}0.5(1\text{-}x)SeO_4{\cdot}0.5x$Cys ($x = 0.5$), interlayer spacing of 7.7–8.5 Å (Fig. 7(b)) and 7.5 to 8.3 Å (Fig. 7(e)) were obtained. They were larger than the d value in pure SeO_4^{2-} systems but smaller than in pure Asp^{2-} and Cys^{2-} systems. In the system of amino acids mixed with CO_3^{2-}, 6.9 to 8.3 Å for Asp^{2-} (Fig. 7(c)) and 6.9 to 8.4 Å for Cys^{2-} (Fig. 7(f)) were predicted in DFT calculation, which

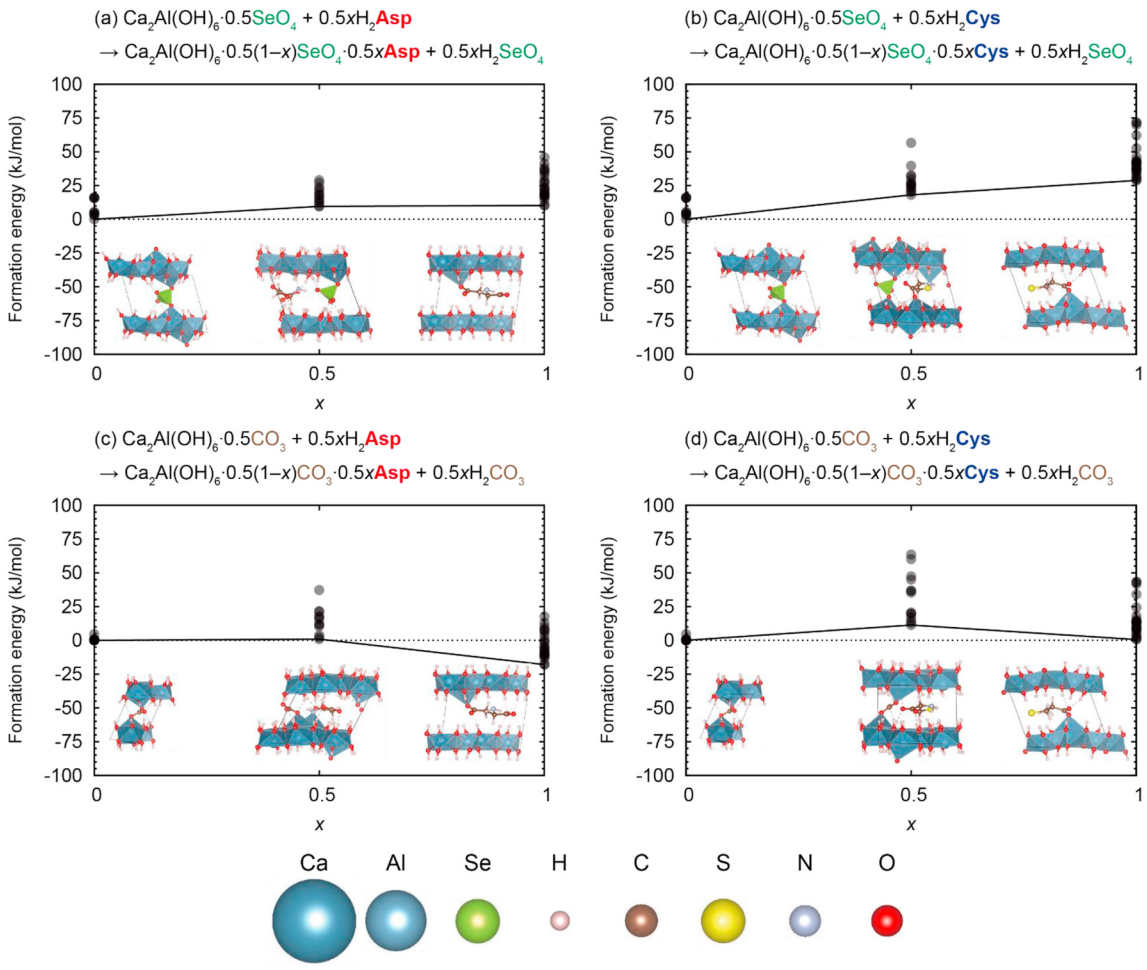

Fig. 6. Formation energies of (a) Ca2Al(OH)6·0.5(1-*x*)SeO4·0.5*x*Asp, (b) Ca2Al(OH)6·0.5(1-*x*)SeO4·0.5*x*Cys, (c) Ca2Al(OH)6·0.5(1-*x*)CO3·0.5*x*Asp, and (d)Ca2Al(OH)6·0.5(1-*x*)CO3·0.5*x*Cys, (x = 0, 0.5, 1) via the ion-exchange reactions of SeO42- and CO32- with Asp2-and Cys2-. The schematic structures with the lowest formation energies are illustrated in the insets.

are a little bit smaller than SeO_4^{2-} mixed with amino acids. This means the SeO_4^{2-} and/or CO_3^{2-} affected the orientations of Asp^{2-} and Cys^{2-} and contributed to the stability of $Ca_2Al(OH)_6{\cdot}0.5(1\text{-}x)CO_3{\cdot}0.5x$Asp ($x$ = 0.5) and $Ca_2Al(OH)_6{\cdot}0.5(1\text{-}x)CO_3{\cdot}0.5x$Cys systems.

Notably, there is a trend that as the interlayer spacing increasing, the formation energy also increased. Here, we selected interlayer spacing with the lowest formation energy in each system to compare with our experimental results in Fig. 5(a)–(c). Taking into account the anhydrous systems in the present simulation, the involvement of water molecules in the real system should affect the interlayer spacing through the host-guest interaction as well as water molecules supply a more flexible space (Yan et al., 2009; Brian et al., 2016). So the computational interlayer values in anhydrous state should be smaller than the experimental results. Therefore, the component (F) in Fig. 5 can be possibly assigned to d_{003} of 7.35 Å in Ca_2Al-LDH(Asp) and 7.20 Å in Ca_2Al-LDH (Cys) in DFT simulation (Fig. 7 (a),(d)). The d_{003} is smaller in component (E) than component (F), so the smaller interlayer spacing values from computational results in Fig. 7 (c) of 7.0 Å and Fig. 7 (f) of 7.3 Å are likely to be assigned. The differences between simulated interlayer spacings and experimentally obtained values are 0.4–0.7 Å. In addition to the water molecules effect, the more complex stacking modes of the layers than simplified unit cell also contributed to the differences. Therefore, based on the above analysis, peak assignments of (E) and (F) in Fig. 5(a), (b), (c) are likely to be Ca_2Al-LDH(Gly/Asp/Cys + CO_3) and Ca_2Al-LDH (Gly/Asp/Cys), respectively. Pure Ca_2Al-LDH(CO_3), where sole CO_3^{2-} is an intercalator in a unit cell of LDH, was excluded from the peak assignments here because the simulated values are too small far from the observed values.

Further, the converged configurations of $Ca_2Al(OH)_6{\cdot}0.25CO_3{\cdot}0.5$Asp ($x$ = 0.5), $Ca_2Al(OH)_6{\cdot}0.25CO_3{\cdot}0.5$Cys ($x$ = 0.5), $Ca_2Al(OH)_6{\cdot}0.5$Asp (x = 1), and $Ca_2Al(OH)_6{\cdot}0.5$Cys (x = 1) showed the possible interaction of Asp^{2-} and Cys^{2-} between Ca_2Al-LDH sheets in Fig. S1. Hydrogen bonds can be formed through carboxyl and amine groups in amino acids to hydroxide layers, and also Ca–O bonds can be created through the oxygen atoms in the carboxyl groups of amino acids with Ca atoms in $[Ca_2Al(OH)_6]^+$. Formation of chemical bonds of Ca–O between the carboxyl groups and Ca atoms in LDH has been predicted by DFT at the first time as long as we know, although it has been predicted by the single crystal XRD. Such a formation of Mg–O chemical bond was not predicted in hydrotalcite (Mg_2Al-LDH) by DFT (Wang et al., 2021), because the atomic size of Ca is enough large to be bared on the hydroxide layers of LDH (Fig. S1(c), (d)). These chemical bonds promoted amino acids molecules oriented in a horizontal direction with their longest axis approximately parallel to the plane of the $[Ca_2Al(OH)_6]^+$. Unexpectedly, direct interaction between amino acids molecules and CO_3^{2-} was not predicted in binary systems of Asp^{2-}-CO_3^{2-} and Cys^{2-}-CO_3^{2-} (Fig. S1(a), (b)). Neither chemical bonds nor hydrogen bonds were projected through thiol groups (-SH) in H_2Cys and the hydroxide layers $[Ca_2Al(OH)_6]^+$ to stabilize the unit cell of $Ca_2Al(OH)_6{\cdot}0.5$Cys (Fig. S1 (d)).

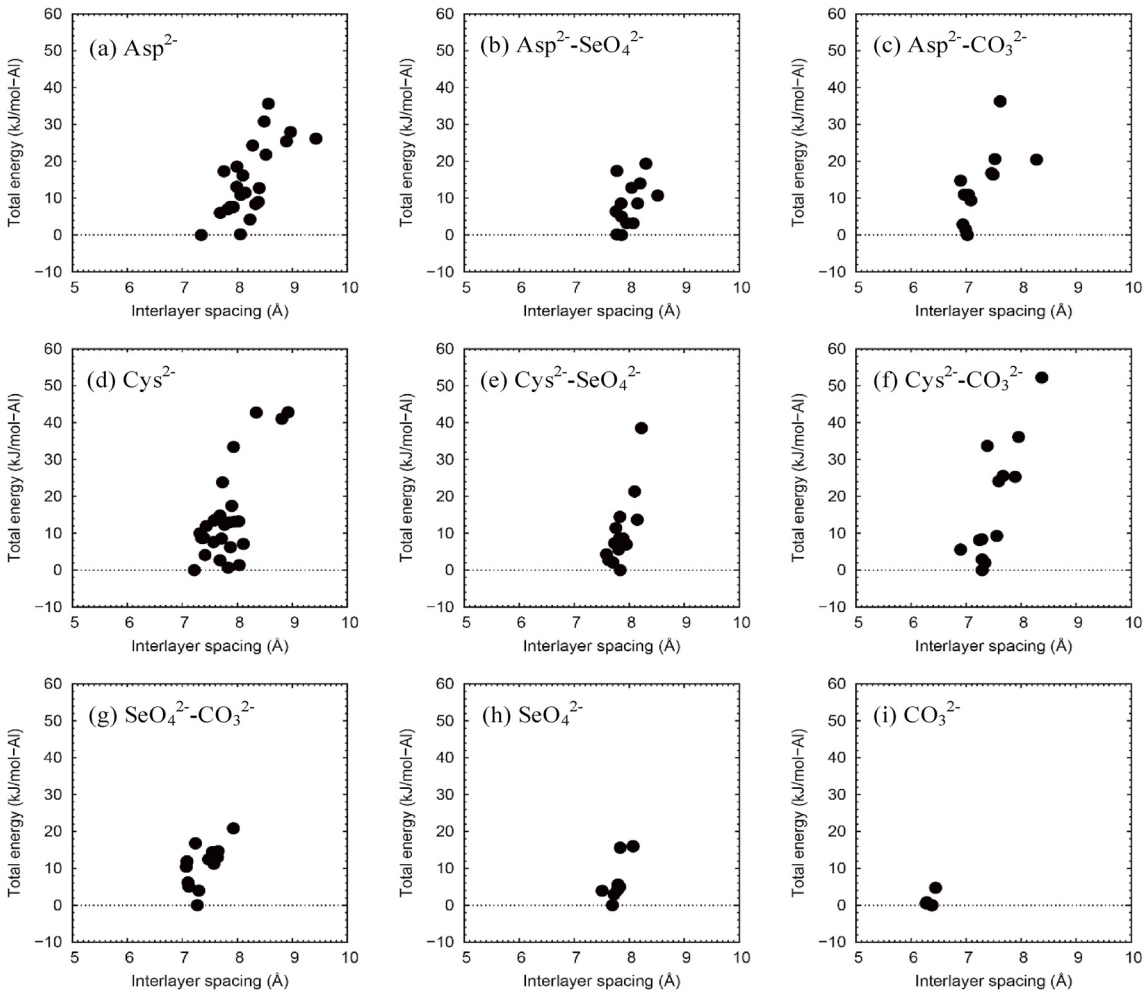

Fig. 7. Total energies plotted against interlayer spacing for Ca2Al-LDH including (a) Asp2-, (b) Asp2–SeO42-, (c) Asp2– CO32-, (d) Cys2-, (e) Cys2– SeO42-, (f) Cys2–CO32-, (g) SeO42– CO32-, (h) SeO42-, (i) CO32-.

3.5. Effect of CO_3^{2-} on the release of SeO_4^{2-}

The changes in relative XRD intensities of each component depending on the sorption densities of amino acids were analyzed to further confirm the peak assignment and SeO_4^{2-} unstabilizing mechanism. To observe the compositional trends of each interlayer anion depending on amino acids loading amounts into Ca_2Al-LDH, relative intensities of d_{003} in XRD (Fig. 5) were plotted against the Q_e values (Fig. 4) as shown in Fig. 8.

HPhe and HTrp were almost not intercalated in the interlayer of Ca_2Al-LDH (Q_e ~0 in Fig. 8(d), (e)). Even at the highest initial concentrations of HPhe and HTrp, SeO_4^{2-} was still maintained 64% in Ca_2Al-LDH (Fig. 3(a)). However, the relative intensities of two configurations (B), (C) of Ca_2Al-LDH(SeO_4) decreased in HGly, H_2Asp, and H_2Cys series as the sorption densities (Q_e) of amino acids increased (Fig. 8(a)–(c)). The relative intensities of Ca_2Al-LDH(amino acid, CO_3) also increased in HGly and H_2Asp series with an increase in Q_e, but not significant in H_2Cys series (Fig. 8(c)). Saturated relative intensities of Ca_2Al-LDH(Asp, CO_3) and Ca_2Al-LDH(Gly, CO_3) reached 79.7% and 76.5%, respectively. This indicates not only amino acids intercalation happened but also CO_3^{2-} was induced to substitute with SeO_4^{2-} from Ca_2Al-LDH. In the H_2Cys series, the relative intensities of Ca_2Al-LDH(Cys, CO_3) was 30%. However, the adsorption amount of H_2Cys showed a little bit larger value than H_2Asp in Fig. 4, therefore, the difference should be caused by the intercalating amount of CO_3^{2-} which is suppressed in the presence of H_2Cys. Therefore, to verify this hypothesis, the formation energies of trinary system Ca_2Al-LDH(SeO_4, CO_3, amino acids) and binary system Ca_2Al-LDH(SeO_4, CO_3) were predicted by DFT simulation, as shown in Fig. 9. The lowest formation energies after CO_3^{2-} ion-exchanged with SeO_4^{2-} in the presence of H_2Asp and H_2Cys were 19.3 and 21.4 kJ/mol (x = 0.5), respectively, which are smaller than 27.6 kJ/mol without amino acids. This means the substitution of CO_3^{2-} with SeO_4^{2-} was slightly more facilitated by the presence of H_2Asp and H_2Cys, furthermore, the presence of H_2Asp was prone to induce more CO_3^{2-} than H_2Cys. This implies that the presence of "reactive" amino acids like HGly, H_2Asp, and H_2Cys may affect the unstabilization of SeO_4^{2-} in Ca_2Al-LDH. Focused on the later faction, H_2Cys relatively stabilized the trinary system Ca_2Al-LDH(SeO_4, CO_3, amino acids), compared with H_2Asp and HGly, to suppress the release of SeO_4^{2-} from Ca_2Al-LDH.

4. Conclusions

In the present study, the stability of hazardous SeO_4^{2-}-bearing hydrocalumite in the presence of different amino acids was investigated by experimental observation integrated with DFT simulation. Main conclusions can be summarized as follows:

(1) In the absence of amino acids, 48.3% of the initially existing SeO_4^{2-} in Ca_2Al-LDH was dissolved, leaving the residual Ca_2Al-LDH where the layer spacing was expanded due to hydration of SeO_4^{2-}.

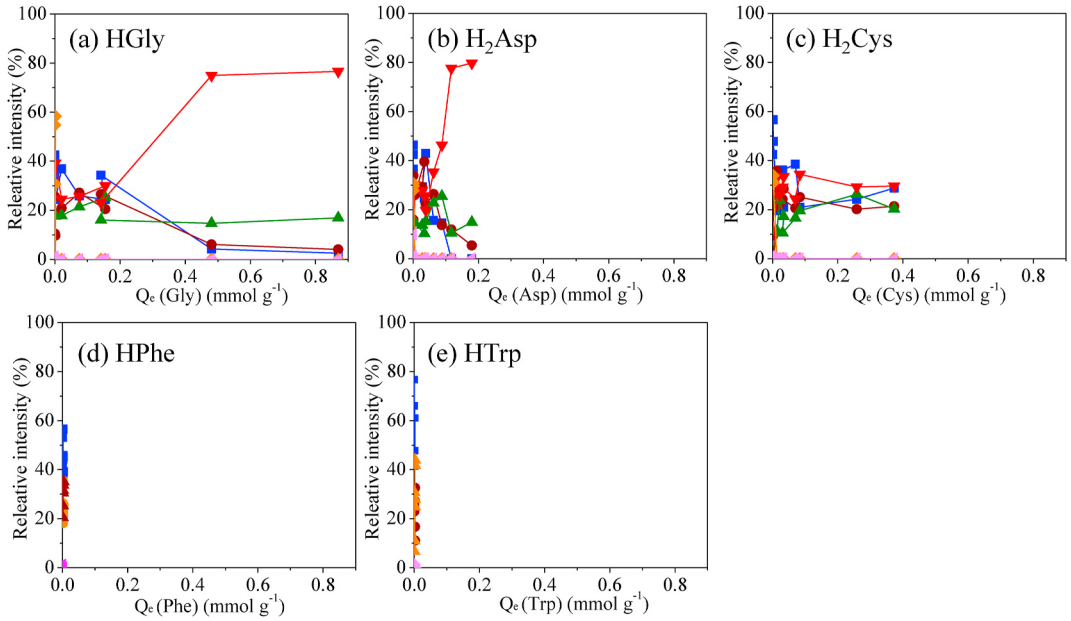

Fig. 8. Plots of relative intensities of each XRD peak components in *d*003 derived from Ca2Al-LDH solid residues after reaction with different concentrations of amino acids against *Qe* values. ♦, Ca2Al-LDH (SeO4, CO3) (*d*003 = 0.793 Å), corresponding to (A) in Fig. 5; ●, Ca2Al-LDH(SeO4) (*d*003 = 0.811 Å), corresponding to (B) in Fig. 5; ■, Ca2Al-LDH(SeO4) (*d*003 = 0.831 Å), corresponding to (C) in Fig. 5; ◀, Ca2Al-LDH(SeO4) (*d*003 = 0.981 Å), corresponding to (D) in Fig. 5; ▼, Ca2Al-LDH (amino acid, CO3) (*d*003 = 7.70 Å), corresponding to (E) in Fig. 5; ▲, Ca2Al-LDH (amino acid) (*d*003 = 7.83 Å), corresponding to (F) in Fig. 5.

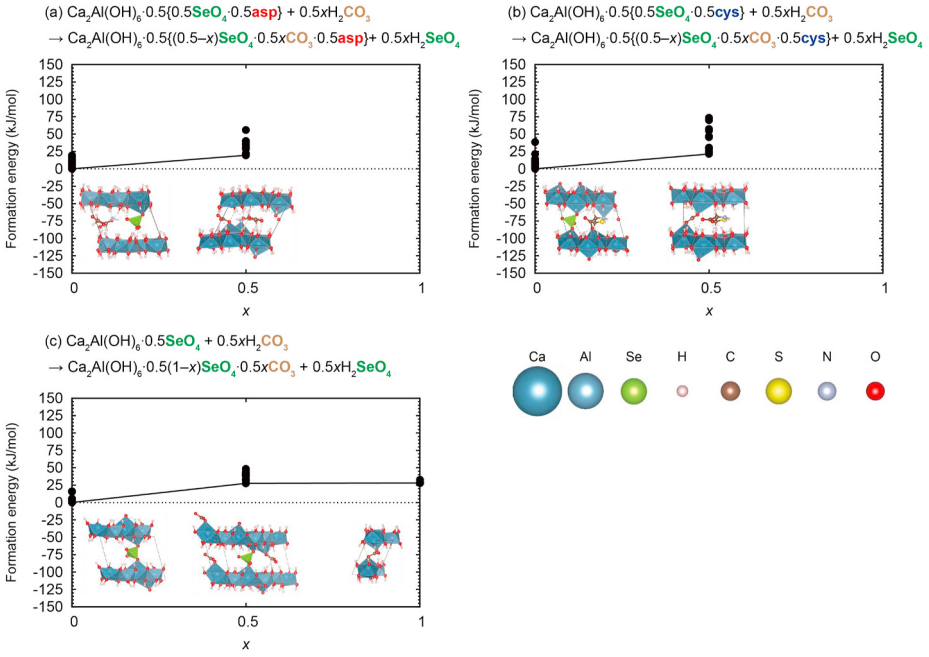

Fig. 9. Formation energies in different systems after ion-exchange of CO32- with SeO42-. (a) Ca2Al(OH)3·0.5(0.5-*x*)SeO4·0.5*x*CO3·0.5Asp, (b) Ca2Al(OH)3·0.5(0.5-*x*)SeO4·0.5*x*CO3·0.5Cys and in the absence of amino acids, (c) Ca2Al(OH)3·0.5(1-*x*)SeO4·0.5*x*CO3 (*x* = 0, 0.5).

(2) Almost no intercalation of HPhe and HTrp happened with Ca_2Al-LDH even though at a high concentration due to their large molecular sizes and hydrophobic properties.

(3) HGly, H_2Asp, and H_2Cys enhanced the release of SeO_4^{2-} from Ca_2Al-LDH. The 003 reflections of XRD patterns for the solid residual Ca_2Al-LDH included the layer spacing derived from selenite with different numbers of hydrated water molecules, carbonate and amino acids, which was supported by DFT calculation. With an increase in sorption densities of amino acids, the relative intensities of d_{003} at large diffraction angles increased. Different trend in the relative intensities was observed in H_2Cys from HGly and H_2Asp series.

(4) DFT calculation predicted that the amino acids molecules are stabilized in the horizontal orientation in Ca_2Al-LDH interlayer through the formation of Ca–O and hydrogen bond between amino acids and hydroxide layer $[Ca_2Al(OH)_6]^+$, and that H_2Asp facilitated the substitution of CO_3^{2-} with SeO_4^{2-} and was prone to more stably co-exist with CO_3^{2-} than H_2Cys. The formation energy of Ca_2Al-LDH was greater in Ca_2Al-LDH(SeO_4, CO_3) than Ca_2Al-LDH(Asp, CO_3) and Ca_2Al-LDH(Cys, CO_3).

(5) Comprehensively, "reactive" amino acids like HGly, H_2Asp, and H_2Cys enhanced the release of SeO_4^{2-} from Ca_2Al-LDH by unstabilization of hydroxide layers and ion-exchange in interlayer.

Declaration of competing interest

The authors declare that they have no known competing financial interests or personal relationships that could have appeared to influence the work reported in this paper.

Acknowledgments

Financial supports were provided to KS and HA by Japan Society for the Promotion of Science (JSPS) KAKENHI research grants (JP19H00883) and Kyushu University Progress 100 (Invitation program for top global researchers) Strategic partnership acceleration (FY2020-2022) and to WM by the China Scholarship Council (201806350035). ID acknowledges support by the DMREF and INFEWS programs of the U.S. National Science Foundation under Grant DMREF-1729338. The computation was carried out using computer resources from the Research Institute for Information Technology at Kyushu University.

Appendix A. Supplementary data

Supplementary data to this article can be found online at https://doi.org/10.1016/j.envpol.2021.117687.

Credit author statements

Mengmeng Wang: Conceptualization, Methodology, Data curation, Formal analysis, Writing – original draft, Writing – review & editing, Validation, Hirofumi Akamatsu: Review & editing, Methodology, Software, Investigation, Validation, Visualization, Ismaila Dabo: Review & editing, Funding acquisition, Supervision, Keiko Sasaki: Conceptualization, Review & editing, Funding acquisition, Resources, Supervision.

References

Baur, I., Johnson, C.A., 2003a. The solubility of selenate-AFt (3CaO· Al_2O_3· 3$CaSeO_4$· 37.5 H_2O) and selenate-AFm (3CaO· Al_2O_3· $CaSeO_4$· xH_2O). Cement Concr. Res. 33, 1741–1748.

Baur, I., Johnson, C.A., 2003b. Sorption of selenite and selenate to cement minerals. Environ. Sci. Technol. 37, 3442–3447.

Baur, I., Keller, P., Mavrocordatos, D., Wehrli, B., Johnson, C.A., 2004. Dissolution-precipitation behaviour of ettringite, monosulfate, and calcium silicate hydrate. Cement Concr. Res. 34, 341–348.

Besse, H.P., Alekseeva, T., Sancelme, M., Delort, A.M., Forano, C., 2009. Atrazine biodegradation modulated by clays and clay/humic acid complexes. Environ. Pollut. 157, 2837–2844.

Blöchl, P.E., 1994. Projector augmented-wave method. Phys. Rev. B 50, 17953–17979.

Cheng, X., Huang, X., Wang, X., Sun, D., 2010. Influence of calcination on the adsorptive removal of phosphate by Zn-Al layered double hydroxides from excess sludge liquor. J. Hazard Mater. 177, 516–523.

Christensen, A.N., Jensen, T.R., Hanson, J.C., 2004. Formation of ettringite, $Ca_6Al_2(SO_4)_3(OH)_{12}$·26$H_2O$, AFt, and monosulfate, $Ca_4Al_2O_6(SO_4)$· 14H_2O, AFm-14, in hydrothermal hydration of Portland cement and of calcium aluminum oxide-calcium sulfate dihydrate mixtures studied by in situ synchrotron X-ray powder diffraction. J. Solid State Chem. 177, 1944–1951.

Chen, H., Sun, Y., Ruan, X., Yu, Y., Zhu, M., Zhang, J., Zhou, J., Xu, Y., Liu, J., Qian, G., 2016. Advanced treatment of stabilized landfill leachate after biochemical process with hydrocalumite chloride (Ca/Al-Cl LDH). Bioresour. Technol. 210, 131–137.

Eklund, L., Persson, I., 2014. Structure and hydrogen bonding of the hydrated selenite and selenate ions in aqueous solution. Dalton Trans. 43, 6315–6321.

Evanko, C.R., Dzombak, D.A., 1998. Influence of structural features on sorption of NOM-analogue organic acids to goethite. Environ. Sci. Technol. 32, 2846–2855.

Fordyce, F.M., 2013. Selenium deficiency and toxicity in the environment. Essentials Med. Geol. 375–416.

Grimme, S., Antony, J., Ehrlich, S., Krieg, H., 2010. A consistent and accurate ab initio parametrization of density functional dispersion correction (DFT-D) for the 94 elements H-Pu. J. Chem. Phys. 132, 154104.

Grimme, S., Ehrlich, S., Goerigk, L., 2011. Effect of the damping function in dispersion corrected density functional theory. J. Comput. Chem. 32, 1456–1465.

Guo, B., Keiko, S., Tsuyoshi, H., 2017. Selenite and selenate uptaken in ettringite: Immobilization mechanisms, coordination chemistry, and insights from structure. Cement Concr. Res. 100, 166–175.

Huang, S., Ming, H., Jinshun, F., Zhong, X., Yang, J., Baiwan, Z., Hua, L., 2009. Assessment of selenium pollution in agricultural soils in the Xuzhou District, Northwest Jiangsu, China. J. Environ. Sci. 21, 481–487.

Kresse, G., Joubert, D., 1999. From ultrasoft pseudopotentials to the projector augmented-wave method. Phys. Rev. B 59, 1758–1775.

Kresse, G., Hafner, J., 1993a. Ab initio molecular dynamics for liquid metals. Phys. Rev. B 47, 558.

Kresse, G., Hafner, J., 1993b. Ab initio molecular dynamics for open-shell transition metals. Phys. Rev. B 48, 13115.

Kresse, G., Furthmüller, J., 1996a. Efficiency of ab-initio total energy calculations for metals and semiconductors using a plane-wave basis set. Comput. Mater. Sci. 6, 15–50.

Kresse, G., Furthmüller, J., 1996b. Efficient iterative schemes for ab initio total-energy calculations using a plane-wave basis set. Phys. Rev. B 54, 11169.

Li, D., Yan, W., Guo, X., Tian, Q., Xu, Z., Zhu, L., 2020. Removal of selenium from caustic solution by adsorption with CaAl layered double hydroxides. Hydrometallurgy 191, 105231.

Li, M., Farmen, L.M., Chan, C.K., 2017. Selenium removal from sulfate-containing groundwater using granular layered double hydroxide materials. Ind. Eng. Chem. Res. 56, 2458–2465.

Liang, X., Butler, E.C., 2010. Effects of natural organic matter model compounds on the transformation of carbon tetrachloride by chloride green rust. Water Res. 44, 2125–2132.

Moon, D.H., Grubb, D.G., Reilly, T.L., 2009. Stabilization/solidification of selenium-impacted soils using Portland cement and cement kiln dust. J. Hazard Mater. 168, 944–951.

Momma, K., Izumi, F., 2011. VESTA 3 for three-dimensional visualization of crystal, volumetric and morphology data. J. Appl. Crystallogr. 44, 1272–1276.

Ong, S.P., Richards, W.D., Jain, A., Hautier, G., Kocher, M., Cholia, S., Gunter, D., Chevrier, V.L., Persson, K.A., Ceder, G., 2013. Python Materials Genomics (pymatgen): a robust, open-source python library for materials analysis. Comput. Mater. Sci. 68, 314–319.

Pye, C.C., Walker, V.E., 2011. Ab initio investigation of the hydration of the tetrahedral perchlorate, perbromate, selenate, arsenate, and vanadate anions. J. Phys. Chem. 115, 13007–13015.

Perdew, J., Burke, K., Ernzerhof, M., 1997. Coupling-constant dependence of atomization energies. Phys. Rev. Lett. 78, 1396.

Perdew, J.P., Burke, K., Ernzerhof, M., 1996. Generalized gradient approximation made simple. Phys. Rev. Lett. 77, 3865.

Perdew, J.P., Ruzsinszky, A., Csonka, G.I., Vydrov, O.A., Scuseria, G.E., Constantin, L.A., Zhou, X., Burke, K., 2008. Restoring the density-gradient expansion for exchange in solids and surfaces. Phys. Rev. Lett. 100, 136406.

Perkins, R.B., Palmer, C.D., 2001. Solubility of chromate hydrocalumite (3CaO· Al_2O_3· $CaCrO_4$· nH_2O) 5-75° C. Cement Concr. Res. 31 (7), 983–992.

Sacerdoti, M., Passaglia, E., 1988. Hydrocalumite from Latium, Italy: its crystal structure and relationship with related synthetic phases. Neues Jahrb für Mineral 462–475.

Santos, R., Tronto, J., Briois, V., Santilli, C., 2017. Thermal decomposition and recovery properties of ZnAl-CO_3 layered double hydroxide for anionic dye adsorption: insight into the aggregative nucleation and growth mechanism of the LDH memory effect. J. Mater. Chem. 5, 9998–10009.

Sipos, P., Pálinkó, I., 2018. As-prepared and intercalated layered double hydroxides of the hydrocalumite type as efficient catalysts in various reactions. Catal. Today 306, 32–41.

Wang, M., Akamatsu, H., Dabo, I., Sasaki, K., 2021. Environmental impact of amino acids on the release of selenate immobilized in hydrotalcite: integrated interpretation of experimental and density-functional theory study. Chemosphere 274, 129927.

Yan, D., Lu, J., Wei, M., Ma, J., Evans, D.G., Duan, X., 2009. A combined study based on experiment and molecular dynamics: perylene tetracarboxylate intercalated in a layered double hydroxide matrix. Phys. Chem. Chem. Phys. 11 (40), 9200–9209.

Yao, W., Wang, J., Wang, P., Wang, X., Yu, S., Zou, Y., Hou, J., Hayat, T., Alsaedi, A., Wang, X., 2017. Synergistic coagulation of GO and secondary adsorption of heavy metal ions on Ca/Al layered double hydroxides. Environ. Pollut. 229, 827–836.

Zhang, M., Reardon, E.J., 2003. Removal of B, Cr, Mo, and Se from wastewater by incorporation into hydrocalumite and ettringite. Environ. Sci. Technol. 37, 2947–2952.